JACS
JOURNAL OF THE AMERICAN CHEMICAL SOCIETY

ARTICLE

pubs.acs.org/JACS

Supported Molecular Iridium Catalysts: Resolving Effects of Metal Nuclearity and Supports as Ligands

Jing Lu,[§,†] Pedro Serna,[§,†] Ceren Aydin,[†] Nigel D. Browning,[†,‡] and Bruce C. Gates*[,†]

[†]Department of Chemical Engineering and Materials Science, University of California-Davis, One Shields Avenue, Davis, California 95616, United States

[‡]Physical and Life Sciences Directorate, Lawrence Livermore National Laboratory, 7000 East Avenue, Livermore, California 94550, United States

Supporting Information

ABSTRACT: The performance of a supported catalyst is influenced by the size and structure of the metal species, the ligands bonded to the metal, and the support. Resolution of these effects has been lacking because of the lack of investigations of catalysts with uniform and systematically varied catalytic sites. We now demonstrate that the performance for ethene hydrogenation of isostructural iridium species on supports with contrasting properties as ligands (electron-donating MgO and electron-withdrawing HY zeolite) can be elucidated on the basis of molecular concepts. Spectra of the working catalysts show that the catalytic reaction rate is determined by the dissociation of H_2 when the iridium, either as mono- or tetra-nuclear species, is supported on MgO and is not when the support is the zeolite. The neighboring iridium sites in clusters are crucial for activation of both H_2 and C_2H_4 when the support is MgO but not when it is the zeolite, because the electron-withdrawing properties of the zeolite support enable even single site-isolated Ir atoms to bond to both C_2H_4 and H_2 and facilitate the catalysis.

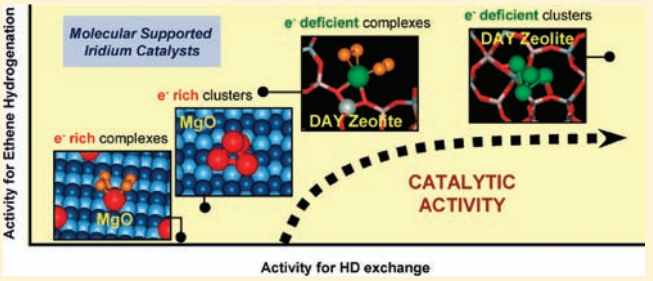

INTRODUCTION

Solid catalysts, the keys to efficient fuel conversion,[1,2] chemical manufacture,[3,4] and pollution abatement,[5] typically consist of nanostructures (metals, metal oxides, or metal sulfides) on porous supports. The performance of a supported catalyst is influenced by the size, shape, and structure of the metal species,[6−8] the ligands bonded to the metal,[9] and the support,[10−13] which itself acts as a ligand when the metal species are small enough to be essentially molecular.[14−17] Resolution of these effects is challenging because the typical solid catalyst consists of highly nonuniform supported species[18,19] on support surfaces that are intrinsically nonuniform. Besides hindering fundamental understanding, the nonuniformity often implies low catalytic selectivity.

In contrast, the typical soluble catalyst, like many metalloenzymes,[20] incorporates a molecular metal complex or cluster with a unique structure that can be determined precisely for fundamental understanding of the catalytic function. Such understanding is similarly achievable with supported catalysts, provided that they are synthesized to incorporate uniform, isolated catalytic structures.[3,20] The challenge begins with the synthesis.[21−25]

Our goals were to investigate a set of catalysts that allow resolution of the roles of the support and the nuclearity of the metal species. We focused on supported catalytic species that are essentially molecular, incorporating controlled numbers of metal atoms and well-defined structures that are (a) stable during catalysis; (b) fully accessible to reactants; (c) present on supports with markedly different reactivities; (d) bonded equivalently to each support; (e) lacking ligands other than the support and reactants; and (f) characterizable by spectroscopy in the functioning state.

The catalysts are mononuclear iridium complexes and clusters consisting of only a few Ir atoms each, supported on solids with widely different properties, highly dehydroxylated MgO, a strong electron-donor ligand, and highly dealuminated HY zeolite (DAY zeolite), an electron-withdrawing ligand.

The structures of the active species were determined by extended X-ray absorption fine structure (EXAFS) and infrared (IR) spectroscopies and high-angle annular dark-field scanning transmission electron microscopy (HAADF-STEM). The catalytic performance was evaluated for the hydrogenation of ethene and for the activation of H_2, the latter indicated by the isotopic exchange reaction of H_2 and D_2.

The spectroscopic characterization of our simple, uniform supported catalysts provides incisive information about the nature and structure of the active sites (metal−ligand, metal−support, and metal−metal interactions) even under working conditions, which allowed identification and quantification of the properties controlling the catalytic activity.

Received: July 12, 2011
Published: August 25, 2011

dx.doi.org/10.1021/ja206486j | J. Am. Chem. Soc. 2011, 133, 16186–16195

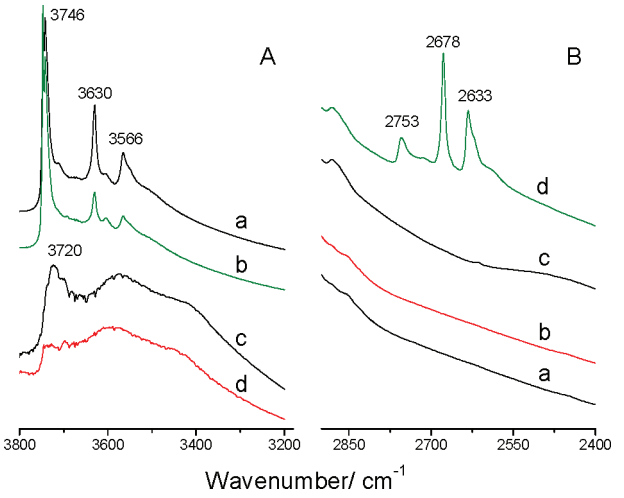

Figure 1. (A) IR spectra (absorbance) in the ν_{OH} stretching region characterizing bare DAY zeolite (a) and MgO (c) and the samples formed by adsorption of $Ir(C_2H_4)_2(acac)$ on this zeolite (b) and on MgO (d). (B) IR spectra in the ν_{OD} stretching region characterizing MgO-supported (a) and DAY zeolite-supported (c) species formed in the reaction of $Ir(C_2H_4)_2(acac)$ with the support (the samples were in flowing helium); and the respective MgO-supported (b) and DAY zeolite-supported (d) samples made by the reaction of the support with $Ir(C_2H_4)_2(acac)$ (the samples were in flowing $H_2 + D_2$ as the catalytic HD exchange reaction took place).

RESULTS

Synthesis of Supported Iridium Complexes. $Ir(C_2H_4)_2$-(acac) (acac is acetylacetonate) was used as the precursor of supported iridium complexes with uniform structures.[26,27] The reaction between $Ir(C_2H_4)_2(acac)$ and the surface of MgO or DAY zeolite, evidenced by IR and EXAFS spectra of the resultant supported species, took place with removal of the acac group and the formation of $Ir(C_2H_4)_2$ bonded to the support through two Ir−O bonds (the support was a bidentate ligand, as expected).[28,29]

Evidence that the $Ir(C_2H_4)_2(acac)$ reacted with the support via the surface OH groups is provided by IR spectra of the samples before and after incorporation of the supported iridium species. Figure 1A shows IR spectra in the ν_{OH} stretching region of bare DAY zeolite, of MgO, and of the respective samples formed by adsorption of $Ir(C_2H_4)_2(acac)$ on each. The bands at 3566 and 3630 cm^{-1} characterizing the DAY zeolite are assigned to acidic OH groups and the band at 3746 cm^{-1} to terminal silanol groups.[30] The reaction of $Ir(C_2H_4)_2(acac)$ with the zeolite led to sharp decreases in the intensities of the 3566 and 3630 cm^{-1} bands characterizing the acidic OH groups, whereas the band at 3746 cm^{-1} characterizing the weakly acidic OH groups remained essentially unchanged. The data thus demonstrate that the $Ir(C_2H_4)_2(acac)$ reacted selectively with the acidic OH groups, that is, those associated with Al sites in the zeolite framework. These results are consistent with the EXAFS data (Table 1), specifically, with the evidence of Ir−Al contributions indicating the bonding of the iridium at Al sites.

The band at 3720 cm^{-1} in the MgO spectrum is assigned to surface OH groups, and the broad unstructured absorption between 3400 and 3600 cm^{-1} is assigned to water molecules on the MgO surface.[31] The reaction of $Ir(C_2H_4)_2(acac)$ with MgO led to a sharp decrease in the intensity of the 3720-cm^{-1} band, indicating that the adsorption involved reaction with the OH groups of this basic surface.

Table 1. EXAFS Data at the Ir L_{III} Edge Characterizing Catalysts Prepared by Reaction of $Ir(C_2H_4)_2(acac)$ with DAY Zeolite and with MgO after Various Treatments

		EXAFS parameters				
support	treatment conditions gas/temperature (K)/time (h)	shell	N	R (Å)	$10^3 \times \Delta\sigma^2$ (Å^2)	ΔE_0 (eV)
DAY zeolite	He/298/1	Ir−Ir	− [a]	− [a]	− [a]	− [a]
		Ir−O	2.0	2.10	0.6	−5.9
		Ir−C	3.9	2.03	9.0	0.26
		Ir−Al	1.0	2.97	8.5	−8.0
		Ir−O_{long}	1.5	3.50	4.8	5.0
MgO	He/298/1	Ir−Ir	− [a]	− [a]	− [a]	− [a]
		Ir−O	2.0	2.00	8.1	−8.0
		Ir−C	4.0	2.12	6.3	−3.1
		Ir−Mg	1.9	3.06	9.5	−5.8
		Ir−O_{long}	3.2	3.70	9.2	−8.0
DAY zeolite	H_2/353/1	Ir−Ir	3.1	2.67	7.9	−4.1
		Ir−O	0.8	2.10	2.9	8.0
		Ir−C	1.6	2.00	14	8.0
		Ir−Al	0.89	2.91	0.3	1.7
		Ir−O_{long}	− [a]	− [a]	− [a]	− [a]
MgO	H_2 /353/1	Ir−Ir	2.9	2.73	4.4	4.2
		Ir−O	1.2	2.33	1.4	8.0
		Ir−C	0.78	2.14	1.5	3.9
		Ir−Mg	2.1	3.17	2.1	−5.5
		Ir−O_{long}	2.8	3.39	1.4	−4.4

Notation: N, coordination number; R, distance between absorber and backscatterer atoms; $\Delta\sigma^2$, Debye−Waller factor; ΔE_0, inner potential correction. Error bounds (accuracies) characterizing the structural parameters are estimated to be as follows: N, ± 20%; R, ± 0.02 Å; $\Delta\sigma^2$, ± 20%; and ΔE_0, ± 20%. [a] Contribution not detectable. Details of the EXAFS fitting are provided in Supporting Information

The IR results showing reactions of the precursor with the OH groups of each support are consistent with the EXAFS data indicating bonding of the iridium in each sample to the surface via Ir−O bonds (Table 1).

Details of the synthesis and interpretation of the spectra are provided in Supporting Information.

The strong influence of the support as a ligand is demonstrated by IR spectra of iridium *gem*-dicarbonyls formed by the almost instantaneous exchange of the initially π-bonded ethene ligands in the supported mononuclear iridium complexes with CO at 298 K. The resultant anchored $Ir(CO)_2$ species were characterized by bands at 1967 and 2051 cm^{-1} when the support was MgO and at 2038 and 2109 cm^{-1} when it was the zeolite (Figure 2). The bands of the MgO-supported complex are red shifted relative to those of $Ir(CO)_2(acac)$ (2002 and 2082 cm^{-1}),[32] whereas those of the isostructural zeolite-supported complex are blue shifted. The shifts confirm the electron-donor character of MgO and the electron-withdrawing character of the zeolite[30,33,34] (Figure 2). Furthermore, the sharpness of the carbonyl bands indicates that the iridium *gem*-dicarbonyls are nearly uniform on each support

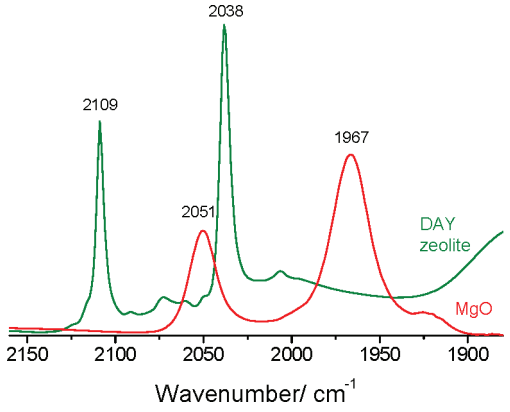

Figure 2. IR spectra (absorbance) in the ν_{CO} stretching region characterizing catalysts formed by adsorption of $Ir(C_2H_4)_2(acac)$ on DAY zeolite and on MgO, after contact with a pulse of CO in flowing helium at 298 K.

and more nearly uniform on the zeolite than the MgO because of its higher degree of crystallinity.[30] Furthermore, the absence of CO peaks other than those characterizing $Ir(CO)_2$ species is consistent with the inference that the sample incorporated mononuclear iridium species and not clusters.[27,35]

Synthesis of Supported Iridium Clusters. Iridium is apparently unique in allowing controlled cluster formation on solid surfaces.[36] Isolated mononuclear iridium complexes undergo selective conversion into nearly uniform ligated clusters, incorporating only several Ir atoms each.[26] On the zeolite support, the clusters formed in high yield in the presence of H_2 at 353 K are Ir_4, as shown by our spectra, which confirm earlier results.[26]

Our data demonstrate analogous chemistry on a support with a much different reactivity, MgO. The isolated $Ir(C_2H_4)_2$ complexes on this support were also converted into clusters approximated as Ir_4 when the sample was treated with H_2 at 353 K for 1 h; the evidence for this conclusion is as follows:

When the supported mononuclear iridium species were treated in flowing H_2 at 353 K and 1 bar, they were characterized by X-ray absorption spectroscopy at the iridium L_{III} edge. The isosbestic points in the X-ray absorption near edge structure (XANES) region (Figure 3) indicate a nearly stoichiometric transformation of one species into another. After 1 h of exposure to H_2, stable clusters had formed on each support, with each Ir atom bonded, on average, to 3 Ir atoms (Table 1), consistent with isolated Ir_4 clusters on the supports. The EXAFS spectra (Figures S14 and S18, Supporting Information) give no evidence of any contribution attributable to high-Z backscatterers at Ir−backscatterer distances >3.2 Å, consistent within error with the absence of clusters large enough to have a second Ir−Ir shell (for details of the EXAFS results and fitting, see Experimental Section).

The H_2-treated samples were imaged by HAADF-STEM to characterize the iridium species. The high-Z contrast images (Figure 4) clearly indicate a predominance of iridium clusters with diameters <1 nm on each support, together with a small number of unconverted mononuclear species (<1% of the total) and a few larger clusters with diameters >1 nm (no cluster was observed with a diameter >1.4 nm). The cluster size distribution determined from the images (Figure 4; see explanation of the method in Supporting Information) indicates that the supported species were nearly uniform and (within error) equivalent on the two supports. The average diameter of the clusters on MgO was 0.66 ± 0.16 nm and that of the clusters on the zeolite 0.61 ± 0.20 nm, both values being

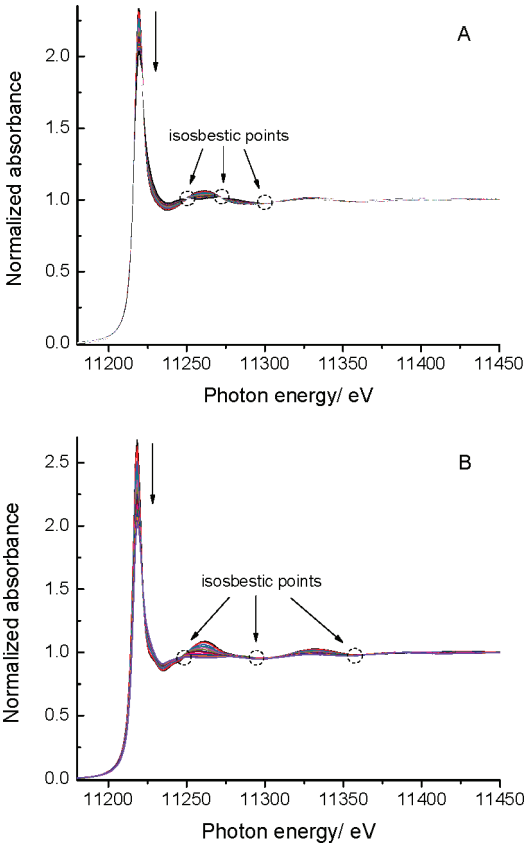

Figure 3. Normalized XANES spectra at the Ir L_{III} edge characterizing the sample formed by the chemisorption $Ir(C_2H_4)_2(acac)$ on (A) DAY zeolite and (B) MgO as cluster formation was occurring at 353 K with the samples in flowing H_2 for 1 h at atmospheric pressure. The isosbestic points indicate the almost stoichiometric conversion of one species to another. The decrease of the white line intensity indicates the reduction of the initially mononuclear iridium species (cluster formation).

close to the diameter determined crystallographically[37] for the Ir_4 tetrahedron in $Ir_4(CO)_{12}$, nearly 0.5 nm. As standard blurring effects in STEM images (associated with electron beam probe size, vibrational instabilities, irradiation effects, off-focus, beam broadening, etc.) are expected to cause a slight overestimation of the sizes of the clusters as well as some broadening of the size distribution, we infer that the images are consistent with the presence of predominantly Ir_4 clusters in both the H_2-treated MgO- and zeolite-supported samples. This inference is in agreement with similar analyses reported by Alley et al.[38]

Catalysis of Ethene Hydrogenation. The performance of each catalyst—iridium complexes and iridium clusters, approximated as Ir_4 on each support, was evaluated by its activity in a tubular packed bed plug-flow reactor at room temperature and atmospheric pressure with the catalyst in contact with flowing $H_2 + C_2H_4$ (2:1 mol ratio) (for details see Table 2, Supporting Information). Neither support alone was catalytically active under the conditions of our experiments.

The catalyst performance data (Table 2), the spectra of the working catalysts, and images of the supported species taken before the samples were used as catalysts indicate that the catalytic activity (measured as the turnover frequency, TOF, the rate per Ir atom) is strongly dependent on the nuclearity of the iridium species and on the nature of the support. The iridium

Table 2. Summary of Structural and Catalytic Performance Data Characterizing Mononuclear Iridium Complexes and Iridium Clusters Approximated as Ir_4 Supported on DAY Zeolite and on MgO

support	form of iridium in catalyst[a]	Ir−Ir coordination number determined by EXAFS data[b]	average cluster diameter determined by HAADF-STEM, nm	HD exchange (%)[d]	catalytic activity for ethene hydrogenation TOF (s^{-1})[e]
MgO	$Ir(C_2H_4)_2$	n.d.	0.3[c]	0.7	0.03
MgO	$Ir_4(C_2H_5)_3$	2.9 ± 0.6	0.66 ± 0.16	3.5	0.18
DAY zeolite	$Ir(C_2H_4)_2$	n.d.	0.3[c]	11.1	0.71
DAY zeolite	$Ir_4(C_2H_5)_6$	3.1 ± 0.6	0.61 ± 0.20	55.5	0.86

[a] Principal form of active sites as determined by IR and EXAFS spectroscopies and HAADF-STEM. Quantification of the number of ligands is based on the average information provided by EXAFS spectroscopy. [b] For the complete set of parameters determined in the EXAFS data fitting, see Table 1. [c] Metal species with diameters <0.3 nm were assigned to isolated Ir atoms. [d] Fractional conversion relative to equilibrium in the exchange of H_2 and D_2 in the presence of C_2H_4. Reaction conditions: 298 K, 1 bar, 0.2 bar H_2, 0.2 bar D_2, 0.2 bar C_2H_4, and balanced with helium. [e] Calculated from differential conversions at time on stream = 0 (extrapolated from the corresponding conversion vs time on stream curves), assuming that that all Ir atoms were accessible to reactants.

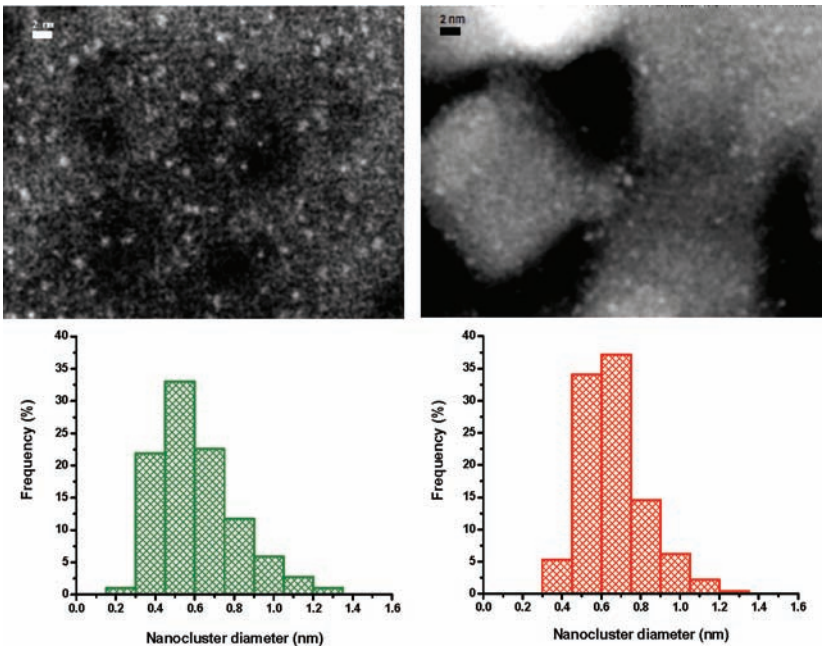

Figure 4. HAADF-STEM images characterizing the catalysts formed by treatment of $Ir(C_2H_4)_2$ species supported on DAY zeolite (left) and MgO (right) as a result of exposure to flowing H_2 at 353 K for 1 h. The images show the presence of nearly uniform iridium clusters approximated as Ir_4 on each support and the absence of iridium clusters >1.4 nm in diameter.

clusters on MgO are more active than the mononuclear iridium complexes on MgO, and the iridium clusters on the zeolite are more active than the mononuclear complexes on the zeolite. However, although the catalytic activity increased 6-fold as mononuclear iridium was converted into clusters when the support was MgO, the corresponding increase was only 1.2-fold when the support was the zeolite. Yet the activity of the iridium complexes on the zeolite was more than 20 times that of the isostructural iridium complexes on MgO, and it was even 4 times that of the iridium clusters on this support.

Thus the data demonstrate a striking support effect, much greater than any yet observed for alkene hydrogenation with catalysts consisting of metal particles having diameters exceeding about 2 nm (these have properties close to those of bulk metal). And this reaction is generally considered a structure-insensitive reaction.[6]

Characterization of Catalysts under Working Conditions. To elucidate the action of the supported iridium complexes and clusters, we investigated them as working catalysts. First, the data was used to characterize the stability of each form of the catalysts under the selected reaction conditions.

In H_2-rich mixtures of $H_2 + C_2H_4$, the iridium clusters retained their nuclearity of approximately 4, as shown by EXAFS spectra. Thus, the effect of ethene as an oxidative fragmentation agent was insufficient to reverse the influence of the H_2 as a reductive cluster-forming agent under these conditions.[27]

The EXAFS data characterizing the mononuclear iridium catalysts at 298 K (with a H_2/C_2H_4 molar ratio of 2) indicate that they also retained the initial nuclearity on each support at this relatively low temperature, while being active for ethene hydrogenation. These data give no evidence of iridium clusters after 2 h of operation in the flow reactor (Tables S1 and S2, Supporting Information). Indeed, the data indicate that even in pure H_2, aggregation of the iridium in the site-isolated complexes did not occur at a significant rate at 298 K (Tables S1 and S2, Supporting Information).[26]

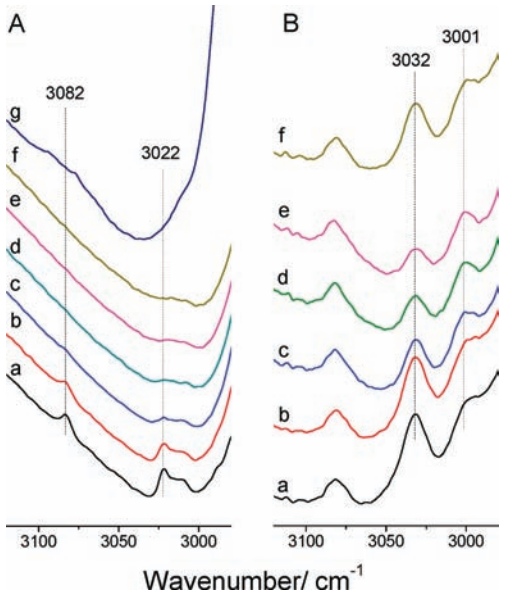

Figure 5. IR spectra (absorbance) in the ν_{CH} region characterizing catalysts in flowing gases at 298 K and 1 bar. (A) DAY zeolite-supported $Ir(C_2H_4)_2$ in helium followed by H_2 for the following times (min): (a) 0, (b) 2, (c) 4, (d) 6, (e) 8, and (f) 10, and (g) in helium followed by $C_2H_4 + H_2$ for 10 min (gas phase purged out with helium before recording of the spectra). (B) MgO-supported $Ir(C_2H_4)_2$ in helium followed by H_2 for the following times (min): (a) 0, (b) 10, (c) 60, (d) 120, and (e) 180, and (f) in helium followed by $C_2H_4 + H_2$ for 10 min (gas phase purged out with helium before recording of the spectra).

In agreement with the EXAFS results, XANES data indicate that in H_2 or $H_2 + C_2H_4$ mixtures at 298 K, the iridium complexes remained mononuclear, evidenced by the markedly different XANES signature of the catalysts treated at 298 K in comparison with those treated in pure H_2 at 353 K (Figures S7 and S8, Supporting Information), which consist of iridium clusters. Nevertheless, as a consequence of the interaction with the reactive atmospheres at the low temperature, subtle changes in the ligand environment of the iridium complexes are evident, and, significantly, these changes are shown to be support dependent, consistent with the roles of the supports as ligands.

The reactivity of the MgO-supported iridium complexes with H_2 is low, as shown by the EXAFS results, which indicate retention of the initial Ir−C coordination number of nearly 4 (for 2 ethene ligands per Ir) in the continuous stream of the reducing agent H_2 at 298 K for >2 h (Tables S1 and S2, Supporting Information). Similar results were obtained with the sample in $C_2H_4 + H_2$, as shown by the EXAFS data (Tables S1 and S2, Supporting Information). These observations are borne out by IR spectra showing that the ethene bonded to isolated Ir atoms, characterized by bands at 3001 and 3032 cm^{-1}, was nearly unchanged with the sample in these reactive atmospheres when the iridium was supported on MgO, even after multiple catalytic turnovers (Figure 5B).

In contrast, the initial Ir−C coordination number of nearly 4, characterizing the sample supported on the zeolite, rapidly decreased to approximately 2 upon contact with either H_2 or $H_2 + C_2H_4$, as a second Ir−C contribution emerged, characterized by an Ir−backscatterer distance and coordination number indicating ethyl ligands σ-bonded to the Ir. The results thus indicate a partial hydrogenation of the ethene and a step toward

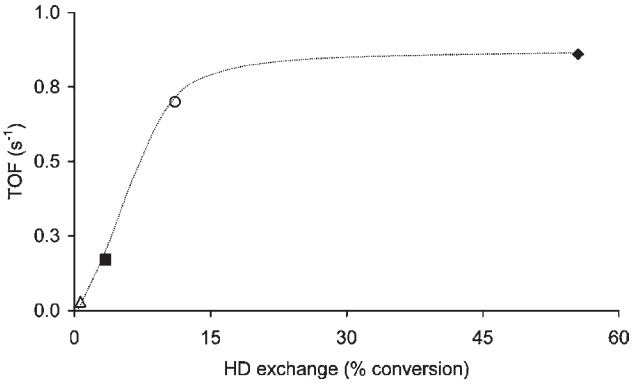

Figure 6. Turnover frequency for the hydrogenation of ethene on various supported iridium catalysts is correlated with the catalytic activity for HD exchange, as measured by the fractional conversion relative to equilibrium for the isotopic exchange of H_2 and D_2: mononuclear iridium species on MgO (△); iridium clusters well approximated as Ir_4 on MgO (■); mononuclear iridium species on DAY zeolite (○); and approximately tetranuclear iridium species on DAY zeolite (♦). The reactions were carried at 298 K and atmospheric pressure.

ethane formation.[26,27] This observation is, moreover, in agreement with IR spectra characterizing the working catalyst, which show a rapid disappearance of the bands ascribed to ethene π-bonded to single Ir atoms, at 3022 and 3088 cm^{-1}, and a concomitant growth of bands at 2964, 2936, 2876, and 2854 cm^{-1}, associated with the formation of ethyl ligands[26] (Figure S3, Supporting Information).

Thus, the spectra give evidence of marked support-dependent differences in the reactivities of the two supported iridium complexes with H_2. To understand the chemistry and expecting that breaking of H−H bonds precedes hydrogenation of the C═C bond, we investigated the dissociation of H_2 on the catalysts by using the HD exchange reaction involving H_2 and D_2.

Catalytic Activity for HD Exchange. In the HD exchange experiments, equimolar mixtures of $H_2 + D_2$ (diluted in helium) flowed through a bed of each catalyst in a tubular reactor operated at 298 K and atmospheric pressure. The concentration of HD in the product was measured by mass spectrometry. Fractional conversions relative to equilibrium were measured in the presence (Figure 6) and in the absence (Figure S22) of C_2H_4.

Significantly, the presence of C_2H_4 cofed with $H_2 + D_2$ (molar ratio $[H_2 + D_2]$: ethene = 2:1) caused a drastic decrease in the rate of HD formation for all four catalysts, indicating competition between the alkene and hydrogen for bonding to the active sites. HD conversions (relative to the equilibrium) ranged from less than 1% for iridium complexes on MgO to 55% for iridium clusters on the zeolite (Figure 6).

■ DISCUSSION

Catalyst Performance. *MgO-Supported Iridium Complexes.* The mononuclear iridium complexes supported on MgO are the least active of our catalysts for ethene hydrogenation (Table 2). The IR spectra characterizing the iridium species probed with CO indicate that the interaction between the mononuclear iridium complexes and the surface of the electron-donating MgO is responsible for an increase in the electron density on the metal.

The turnover frequency characterizing this catalyst for ethene hydrogenation is similar to the value reported previously, but this statement is inexact because the reaction conditions were not the same.[28] The relatively low catalytic activity is consistent with the

observation that the initial ethene ligands of the MgO-supported iridium complexes are rather stable in a stream of H_2 at 298 K and 1 bar (Figure 5B), under conditions for which the rate of activation of H_2 on the metal, indicated by the results of the HD exchange experiments, was shown to be very low.

These results together with the fact that in mixtures of H_2 + C_2H_4 (during catalysis) almost every isolated Ir atom was bonded to two ethene ligands, as shown by the EXAFS (Table S2, Supporting Information) and IR (Figure 5B) spectra, suggest that ethene is more facilely adsorbed on the isolated Ir atoms than H_2. Indeed, the HD exchange data showed that the fractional conversion of H_2 relative to equilibrium dropped almost two orders of magnitude in the presence of relatively low gas-phase concentrations of C_2H_4, evidencing a strong inhibition of H_2 dissociation by C_2H_4 (Figure S22, Supporting Information).

This result is contrasted with the observation that the hydrogenation of ethene catalyzed by $IrCl(PPh_3)_3$ complexes in solution, the iridium analogue of Wilkinson's rhodium complex, is not limited by H_2 dissociation but by the formation of stable $IrClH_2(PPh_3)_3$ species that do not activate the alkene.[40]

On the basis of our results, we infer that the activity of the catalyst for alkene hydrogenation could be increased: (a) if each active site comprised several Ir atoms that could take on separate functions, including the activation of both reactants, and/or (b) if the bonding of the alkene and hydrogen to the isolated Ir atoms could be optimized.

MgO-Supported Iridium Clusters. In agreement with inference (a), the activity of the MgO-supported catalyst for hydrogenation of ethene was markedly boosted when the isolated iridium complexes were converted into iridium clusters by treatment with H_2. Remarkably, the increase in the catalytic reaction rate occurred concomitantly with an increase in the reactivity for dissociation of H_2, indicated by the catalytic HD exchange data (Table 2, Figure 6). These results suggest that the activation of H_2 on the MgO-supported iridium complexes is rate determining in the catalytic hydrogenation.

The foregoing result agrees with a broadly observed pattern, indicating that noble metal clusters are more active as alkene hydrogenation catalysts than mononuclear complexes of the same metal (and the turnover frequency characterizing this catalyst for ethene hydrogenation is similar to the value reported previously.[36] The higher activity of the clusters is usually attributed to the more rapid activation of H_2 on metal clusters (or surfaces) than on mononuclear metal complexes.[41,42]

However, more significantly, the HD exchange data indicate that the inhibition of H_2 activation by ethene is less significant (~3 times less) when the iridium is present in clusters rather than isolated complexes (Figure S22, Supporting Information), a result that supports the hypothesis that multiple neighboring Ir atoms cooperate in the simultaneous activation of H_2 and C_2H_4, boosting the catalytic hydrogenation activity (at least when the rate is limited by the adsorption of one of the reactants, as we infer for the MgO-supported complexes).

Zeolite-Supported Iridium Complexes. Beyond the effect of metal nuclearity, our data demonstrate that the activity of mononuclear iridium complexes can be enhanced by taking advantage of the properties of the support as an activating ligand,[10] as in homogeneous organometallic catalysis.[43−45]

The effect of acidic zeolite supports on the catalytic performance of metal species has been investigated for metal nanoparticles,[14,46−48] but a resolution of the effects of metal−support interactions and nanoparticle shape and size has remained elusive.[6,15,47] Our results address this point unambiguously and unprecedentedly for catalysts with well-defined structures.

The data (Table 2, Figure 6) show that the activity of the electron-rich mononuclear iridium complexes on MgO increases >20-fold when the zeolite replaces MgO as a support, as the acidic support surface, acting as an electron-withdrawing macroligand, creates electron-deficient iridium complexes (evidenced by IR spectra of supported $Ir(CO)_2$ species, Figure 2).

Remarkably, the activity of the isolated iridium complexes on the electron-withdrawing zeolite support, requiring each Ir atom to activate both H_2 and C_2H_4, is more than four times greater than the activity of iridium clusters on the electron-donating MgO, whereby neighboring Ir atoms are positioned to take on separate functions in the catalysis.

The high ethene hydrogenation activity of the zeolite-supported iridium complexes matches the high activity of this catalyst for H_2 dissociation (Figure 6, Table 2).

The IR spectra provide a confirmation of the reactivity of the zeolite-supported iridium complexes for hydrogen activation. The spectra of the sample in a mixture of H_2 and D_2 include not just the bands characterizing OH groups on the zeolite surface (at 3566, 3630, and 3746 cm^{-1}, these were lower in intensity than those of the sample before contact with the H_2-D_2 mixture) but also new bands that appeared at 2633, 2678, and 2753 cm^{-1} (Figure 1B). These new bands are assigned to OD species on the zeolite, as their frequencies match well the values expected when H is replaced by D according to the Hooke's law assumption.[49] We attribute this observation to the spillover of deuterium from the metal complexes to the zeolite surface.[50] Furthermore, as shown in Figure 1B, no shifts of the OH bands occurred when MgO supported iridium complexes were treated under identical conditions, consistent with its slow HD exchange rate.

Accordingly, the IR and EXAFS spectra of the zeolite-supported iridium complexes in H_2 at room temperature (Figure S2, Supporting Information) show that the ethene ligands initially π-bonded to the Ir centers reacted readily to form partially hydrogenated intermediates (ethyl).

These data demonstrate that the formation of ethyl ligands on the zeolite-supported iridium complexes occurs facilely, faster than the reductive elimination of the catalytic reaction product ethane and adsorption of alkene molecules from the gas phase. Thus, these results imply that the reaction rate is not determined by the H_2-dissociation rate when the catalyst is the zeolite-supported iridium complex.

Zeolite-Supported Iridium Clusters. In agreement with the inference that the rate of the ethene hydrogenation reaction is not determined by the H_2 activation on electron-deficient iridium complexes on the zeolite, our data show that the reaction rate was not affected substantially by the further enhancement of the H_2-dissociation rate by generation of iridium clusters on the zeolite (Table 2, and Figure 6). Thus, the presence in this form of the catalyst of neighboring metal centers to facilitate activation of H_2 is of only minor importance.

Effect of Support vs Effect of Metal Nuclearity. In summary, our results demonstrate how the performance of a supported metal catalyst can be tuned by inducing changes either in the nature of the metal−support interactions (metal−ligand bonding) or the nuclearity of the metal species. When each active site consists of at most a few metal atoms, the prerequisite that each of the reactants (H_2 and C_2H_4 in our case) must simultaneously interact with the active sites to facilitate catalysis is not in general easily met; a suitable balance is necessary to prevent the

Scheme 1. Reaction Pathway for the Hydrogenation of Ethene on Iridium Complexes Supported on DAY Zeolite (left) and MgO (right), as Inferred from EXAFS and IR Spectra Characterizing the Active Sites in Reactive Atmospheres of $C_2H_4 + H_2$ at 298 K and 1 bar[a]

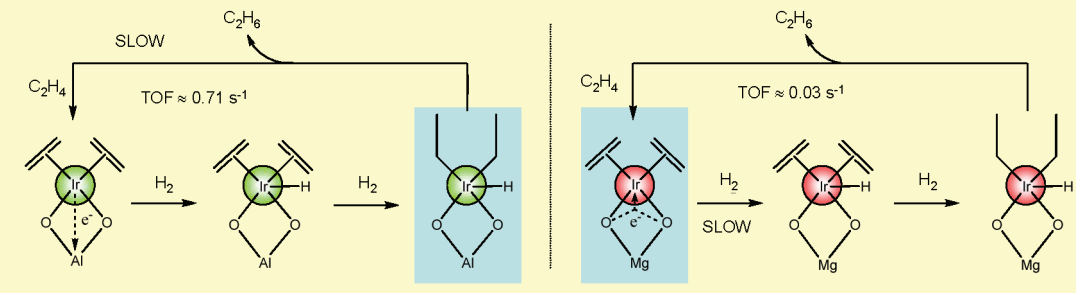

[a] The iridium sites are color coded to indicate electron deficiency of the metal on the surface of the zeolite (left, green) and electron enrichment on the surface of MgO (right, red). Shadowed species correspond to the stable reaction intermediates, as inferred from EXAFS and IR spectra, which depend on the support.

possibility that one of the reactants swamps the catalytic sites and impedes the bonding of the other reactant that is necessary for completion of a catalytic cycle. This generalization is well established in molecular homogeneous catalysis.[40] Our contribution here, beyond the illustration of its validity in surface catalysis, is the understanding of and demonstration of how to facilitate the optimization of catalytic sites on solid supports; the site isolation of the catalytic sites is important to the success of the approach.

Our data show that the effect of the metal nuclearity on the catalytic activity of iridium for ethene hydrogenation is strongly dependent on the nature of the metal−support interaction, being much more important when the iridium sites are electron-rich on the basic MgO than when they are electron deficient on the acidic zeolite. The data show that electron enrichment of the iridium is responsible for a diminution of the capacity of the iridium to react with and form ligands from H_2 and C_2H_4 simultaneously, and in this case, the adsorption of the latter hinders the activation of H_2. Accordingly, high activities for ethene hydrogenation on MgO-supported catalysts require the presence of several neighboring Ir atoms that can take on separate functions in the catalytic reaction.

However, as in numerous examples of metal-complex catalysis in solution, the performance of essentially molecular species is influenced not only by the characteristics of the metal−metal framework but also by the ligands that enable the metal centers to facilely enter into the catalytic cycle and allow the turnover. For example, in alkene hydroformylation catalysis by unsupported organorhodium complexes, the reaction rate is usually increased by the use of electron-withdrawing ligands that modify the metal centers (e.g., rates are higher with phosphite ligands than with phosphane ligands).[51] Our data show that even isolated Ir atoms, only slightly active on the surface of MgO, can provide high activities for alkene hydrogenation when the ligand that is the solid support is electron withdrawing, because then the simultaneous bonding of both hydrogen and C_2H_4 is allowed in a balance that facilitates rapid turnover.

Influence of Metal−Support Interactions on Ethene Hydrogenation Reaction Pathway. Besides showing that the support can have a stronger influence on the rate of the catalytic hydrogenation of ethene than the metal nuclearity, the results presented here show that uniform and structurally simple supported metal complexes offer unique opportunities for understanding the fundamentals of catalysis, as the active sites can be tuned systematically and characterized incisively, with the characterizations leading to identification of the ligands bonded to the metal during catalysis.

In flowing mixtures of H_2 and C_2H_4, the MgO-supported iridium complexes, as shown by the IR and EXAFS spectra, are predominantly $Ir(C_2H_4)_2$ (Figure 5 and Table S2, Supporting Information), which we infer to be the most stable reaction intermediate. Moreover, the fact that these species activate H_2 only slowly (Table 2) is consistent with additional IR spectra, giving no evidence of iridium-hydride bands with the sample in H_2 at 298 K and 1 bar. Accordingly, we infer that although iridium hydride species are expected to be reaction intermediates in the ethene hydrogenation reaction,[44] these species are a small minority under our conditions.

In contrast, the EXAFS and IR spectra characterizing the zeolite-supported iridium complex catalyst in the working state demonstrate that $Ir(C_2H_5)_2$ is the predominant reaction intermediate (Figure 5, Tables S1, Supporting Information). The observations indicate that the conversion of ethene into ethyl ligands occurs facilely, consistent with the fast dissociation of H_2 determined by the HD exchange experiments (Table 2). The facile formation of iridium hydride(s) is demonstrated by the observation of an intense band at 2068 cm^{-1} in the IR spectra characterizing the zeolite-supported complexes in the presence of pure H_2 at 298 K and 1 bar. The frequency of this band and its shift to 1509 cm^{-1} when H_2 is replaced by D_2 in the gas phase (Figure S23, Supporting Information) demonstrate the formation of iridium hydride species.[49,52−54]

These observations, together with the inference that the reaction rate is limited by H_2 activation when iridium is electron-rich on the surface of MgO, as previously discussed, but not when it is electron-deficient on the surface of the zeolite, allow us to propose a simplified reaction scheme summarizing the data and highlighting the important differences in the mode of catalytic action of the MgO- and zeolite-supported iridium complexes (Scheme 1). In this scheme, elementary steps for the C=C hydrogenation are included according to the Horiuti−Polanyi mechanism, which is consistent with all our observations.[55]

Our results demonstrate that solid supports acting as macroligands exert a significant influence on the catalytic properties of essentially molecular metal species. These effects may be comparable in magnitude to the effects observed with organic ligands

in solution catalysis. The depth of understanding of such effects in surface catalysis can nearly match that in molecular homogeneous catalysis when the supported metal species are precisely synthesized to be simple and uniform. Thus, we anticipate that our conclusions about the action of essentially molecular supported catalysts may extend to a much larger family of metal species on solid surfaces, but we emphasize that these effects will decline in importance as the metal species become larger, approaching bulk metals. The foundation underlying catalysis by supported species as small as ours is essentially molecular chemistry, whereas that underlying catalysis by supported particles with the properties of bulk metals is primarily single-crystal surface science.

■ CONCLUSIONS

In catalysis by supported metal species, both the support and the nuclearity of the metal in the catalytic sites are important in regulating the catalytic properties. The activity for ethene hydrogenation of supported iridium complexes is boosted in two ways, which are resolved by the data presented here: (a) By the electron-withdrawing zeolite support acting as a ligand that modifies the electron density on the metal center for efficient activation of C_2H_4 and H_2 simultaneously. (In contrast, iridium complexes supported on MgO are electron rich and are nearly coordinatively saturated, with ethene ligands occupying bonding sites and hindering the activation of H_2.) (b) By conversion of the mononuclear iridium complexes into small clusters that provide neighboring iridium sites where both coordination and activation of both ethene and hydrogen take place.

■ EXPERIMENTAL METHODS

Sample synthesis and handling were performed with the exclusion of moisture and air. The zeolite (Zeolyst International, CBV760; Si:Al atomic ratio ≅ 30) was calcined in O_2 at 773 K for 4 h and evacuated for 16 h at 773 K. MgO (EM Science, surface area, 70 $m^2\ g^{-1}$) was mixed with deionized water to form a paste, which was dried overnight in air at 393 K. The resultant solid was ground and treated in O_2 as the temperature was ramped linearly from room temperature to 973 K and then held for 2 h. $Ir(C_2H_4)_2(acac)$[56] reacted at 298 K with the treated zeolite or MgO in a slurry in dried, deoxygenated *n*-pentane. The iridium content of each resultant powder was 1 wt %.

X-ray absorption spectra were recorded at X-ray beamlines 10-ID (MR-CAT) and 9-BM at the Advanced Photon Source at Argonne National Laboratory. The cryogenic double-crystal Si(111) monochromator was detuned by 20−25% at the Ir L_{III} edge to minimize effects of higher harmonics in the X-ray beam. The samples were loaded into a flow-through cell,[57] which was sealed in an atmosphere of N_2.

A Bruker IFS 66v/S spectrometer with a spectral resolution of 2 cm^{-1} was used to collect transmission IR spectra of power samples.

Details of the spectroscopy experiments are given in Supporting Information.

HAADF-STEM images of the samples were obtained with a JEOL JEM-2100F electron microscope equipped with an FEG, operating at 200 kV with a CEOS hexapole probe (STEM) aberration corrector. The images were captured with an HAADF detector with a collection semiangle of 75−200 mrad and a probe convergence semiangle of 17.1 mrad. Size measurement was done on the intensity profiles across clusters in STEM images obtained by using DigitalMicrograph. The profiles then were fitted to a Gaussian distribution function by using Origin Pro, and full width half-maximum values were determined and are reported as diameters of the clusters.

Ethene hydrogenation catalysis was carried out in a conventional laboratory once-through tubular plug-flow reactor at 298 K and 1 bar. The catalyst (30 to 150 mg per sample) was diluted with 10 g of inert, nonporous α-Al_2O_3 and loaded into the reactor in an inert-atmosphere glovebox. The feed partial pressure was 333 mbar of C_2H_4 and 666 mbar of H_2, with a total flow rate of 60 mL(NTP)/min. Products were analyzed by gas chromatography. The ethene conversions were <5%, and the reactor was approximated as differential, determining reaction rates directly.

The isotopic H_2/D_2 exchange reaction experiments were similarly carried out in a tubular plug-flow reactor at 298 K and 1 bar. Measurements were made with H_2 and D_2 feed partial pressures of 200 mbar each, with an additional 200 mbar of C_2H_4 in some experiments, balanced in helium, and with a total flow rate of 100 mL(NTP)/min. Mass spectra of the gases introduced into the flow system and the products of the reaction were measured with an online Balzers OmniStar mass spectrometer.

EXAFS Data Analysis. The X-ray absorption edge energy was calibrated with the measured signal of a platinum foil (scanned simultaneously with the sample) at the Pt L_{III} edge, which was taken to be the inflection point at 11 564 eV. The data were normalized by dividing the absorption intensity by the height of the absorption edge.

Analysis of the EXAFS data was carried out with the software ATHENA of the IFEFFIT[58,59] package and the software XDAP developed by Vaarkamp et al.[60] Each spectrum that was subjected to analysis was the average between 2 to 4 consecutive spectra. ATHENA was used for edge calibration, deglitching, and data normalization. XDAP was used for background removal, normalization, and conversion of the data into an EXAFS (χ) file. A difference-file technique was applied with XDAP for determination of optimized fit parameters. Each spectrum was processed by fitting a second-order polynomial to the pre-edge region and subtracting this from the entire spectrum. The functional that was minimized and the function used to model the data are given elsewhere.[61] The background was subtracted by using cubic spline routines. Reference backscattering phase shifts were calculated with the software FEFF7[62] from crystallographic data. $Ir(C_2H_4)_2(acac)$[56] was used for $Ir-O_{support}$, Ir−C, $Ir-O_{long}$, and $Ir-C_{long}$ contributions; Ir−Al alloy[63] was used for the Ir−Al contribution; Ir−Mg alloy[63] was used for the Ir−Mg contribution; and iridium metal[63] was used for Ir−Ir contributions. Iterative fitting was done in *R* (distance) space with the Fourier-transformed χ data until optimum agreement was attained between the calculated k^0-, k^1-, k^2-, and k^3-weighted EXAFS data and each postulated model (*k* is the wave vector). The number of parameters used in the fitting was always less than the statistically justified number, computed with the Nyquist theorem:[64] $n = (2\Delta k\Delta r/\pi) + 1$, where Δk and Δr, respectively, are the *k* and *r* ranges used in the fitting.

Detailed Example of EXAFS Data Fitting. Described here, as an example, is the detailed analysis carried out for the data characterizing the MgO-supported iridium complex at the end of the H_2 treatment at 353 K. Various combinations of plausible absorber−backscatterer contributions ($Ir-O_{support}$, Ir−C, Ir−Mg, $Ir-O_{long}$, Ir−Ir (first shell), and Ir−Ir (second shell) were fitted initially, leading to a narrowed list of candidate models on the basis of the goodness of fit, specifically including the goodness of the overall fit in both *k* and *R* spaces. Further evaluation was carried out by comparing the fits of individual contributions obtained by a "difference file" method that is illustrated below.

The detailed fitting parameters determined for the final three candidate models are summarized in Table S3, Supporting Information. We emphasize that attempts were made to exclude Ir−Ir contributions in the fitting (in case the catalyst had still been mononuclear), but no models could be found to give nearly satisfactory overall fits or satisfactory goodness of fit values in this example.

Each of the three models found to be most successful in fitting the data included an Ir−Ir contribution. Both models I and II have only one Ir−Ir contribution, and they differ only with regard to the presence of an

Ir−O_{long} contribution (this is one with an Ir−O distance longer than a bonding distance). A summary of the models is given in Table S3, Supporting Information. To test whether clusters larger than Ir_4 were formed, in model III we introduced a second Ir−Ir contribution. Models I and III differ only in the replacement of an Ir−Ir second-shell contribution with an Ir−O_{long} contribution.

Each of these models provides a good overall fit of the data in *k* space and a good fit with respect to the goodness of fit value (Table S3, Supporting Information). However, a representation of the data in *R* space (Figures S18−S20, Supporting Information) shows that the overall fit represents the data well up to *R* = 3.8 Å for model I, whereas for models II and III the fits between *R* = 3.0 and 3.8 Å are less satisfactory, which is an indication of either a missing contribution or a wrong contribution that was included in the fit at approximately that distance. As shown in Table S3, Supporting Information, in model II, there is no Ir−backscatter shell at a distance between 2.8 and 3.8 Å, which explains the inadequate fit in *R* space in that region. An additional Ir−O_{long} shell at a distance of 3.40 Å was introduced into model I, which significantly improved the overall fit in *R* space. However, the addition of a second Ir−Ir shell at a distance of 3.72 Å (within the range of a typical Ir−Ir second-shell distance) introduced an additional peak at approximately 3.7 Å in the plot of data in *R* space, which did not fit the data. Moreover, model III gives a relatively high value for goodness of fit compared with models I and II, indicating that Model I is a better representation of the experimental results than the other models.

To further examine the fitting parameters and compare candidate models, a difference-file technique was applied by using the software XDAP,[60] in which the calculated EXAFS contribution from each individual Ir−backscatterer contribution was compared with the data in *R* space (calculated from subtracting all the other calculated Ir−backscatterer contributions from the overall observed contributions). The best model should give not only good overall fits in both *k* space and *R* space but should also provide a good fit in each of the individual contributions. Comparing models I and II, we see that all the individual shells fit better for model I, especially the Ir−Mg contribution. In model III, as shown in Figure S20, Supporting Information, it is clear that the second Ir−Ir shell does not fit the data well at all. Furthermore, the fits with all the other shells are markedly worse than for models I or II. Thus, there is strong evidence that the supported iridium clusters, on average, are not larger than Ir_4.

On the basis of the evaluation of overall fits in *k* and in *R* space, the goodness of fit values, and the individual fits in *R* space, we select model I as the one providing the best fit of the data. This model indicates an Ir−Ir coordination number of 2.9, corresponding to a tetrahedral Ir_4 cluster (and we emphasize that the other, less satisfactory, models also indicated such small iridium clusters, with Ir−Ir coordination numbers of 3.0 and 2.9, respectively, for models II and III).

EXAFS analyses for other samples were carried out in a fashion similar to that described above. We emphasize that attempts were made to include Ir−Ir contributions (to test for the presence of clusters) in the fits of the data characterizing all the samples, but for the initially prepared sample and samples that were treated at 298 K, no models were found (with the fitting done with each of the *k* weightings 1−3) to give nearly satisfactory overall fits or physically appropriate fit parameters. We also emphasize that the contributions are weak for those Ir−backscatterer contributions at distances longer than bonding distances, and it was therefore difficult to distinguish one of these weak contributions from another (e.g., Ir−Mg and Ir−O_{long}). Thus, those contributions are assigned only tentatively, and the errors characterizing those shells are greater than the errors stated for other shells.

■ ASSOCIATED CONTENT

Supporting Information. Further details of the experimental methods are provided in the Supporting Information. This material is available free of charge via the Internet at http://pubs.acs.org.

■ AUTHOR INFORMATION

Corresponding Author
bcgates@ucdavis.edu

Author Contributions
§These authors contributed equally.

■ ACKNOWLEDGMENT

This research was supported by the DOE (Basic Energy Sciences, Contract FG02-04ER15513) (J.L. and C.A.). The research leading to these results has received funding from the European Union Seventh Framework Programme (FP7/2007-2013) under grant agreement no. PIOF-GA-2009-253129 (P.S.) We acknowledge beam time and the support of the DOE Division of Materials Sciences for its role in the operation and development of beamlines MR-CAT and Sector 9 at the Advanced Photon Source at Argonne National Laboratory. We thank Rodrigo Lobo-Lapidus, Tomohiro Shibata, and Trudy Bolin for valuable support.

■ REFERENCES

(1) Huber, G. W.; Iborra, S.; Corma, A. *Chem. Rev.* **2006**, *106*, 4044.
(2) Ratnasamy, C.; Wagner, J. P. *Catal. Rev. Sci. Eng.* **2009**, *51*, 325.
(3) De Vos, D. E.; Dams, M.; Sels, B. F.; Jacobs, P. A. *Chem. Rev.* **2002**, *102*, 3615.
(4) Blaser, H. U.; Malan, C.; Pugin, B.; Spindler, F.; Steiner, H.; Studer, M. *Adv. Synth. Catal.* **2003**, *345*, 103.
(5) Ishida, T.; Haruta, M. *Angew. Chem., Int. Ed.* **2007**, *46*, 7154.
(6) Boudart, M.; Djéga-Mariadassou, G. *Kinetics of Heterogeneous Catalytic Reactions*; Princeton University Press: Princeton, NJ, 1984.
(7) Boudart, M. *Adv. Catal.* **1969**, *20*, 153.
(8) Lee, I.; Delbecq, F.; Morales, R.; Albiter, M. A.; Zaera, F. *Nat. Mat* **2009**, *8*, 132.
(9) Carboni, S.; Gennari, C.; Pignataro, L.; Piarulli, U. *Dalton Trans.* **2011**, *40*, 4355.
(10) Stair, P. C. *Nat. Chem.* **2011**, *3*, 345.
(11) Tauster, S. J.; Fung, S. C.; Garten, R. L. *J. Am. Chem. Soc.* **1978**, *100*, 170.
(12) Tauster, S. J.; Fung, S. C.; Baker, R. T. K.; Horsley, J. A. *Science (Washington, DC, U.S.)* **1981**, *211*, 1121.
(13) Coq, B.; Figueras, F. *Coord. Chem. Rev.* **1998**, *178−180*, 1753.
(14) Sachtler, W. M. H.; Zhang, Z. *Adv. Catal.* **1993**, *39*, 129.
(15) Stakheev, A. Y.; Kustov, L. M. *Appl. Catal., A* **1999**, *188*, 3.
(16) Fujdala, K. L.; Tilley, T. D. *J. Catal.* **2003**, *216*, 265.
(17) Vayssilov, G. N.; Lykhach, Y.; Migani, A.; Staudt, T.; Petrova, G. P.; Tsud, N.; Skála, T.; Bruix, A.; Illas, F.; Prince, K. C.; Matolín, V.; Neyman, K. M.; Libuda, J. *Nat. Mat.* **2011**, *10*, 310.
(18) Thomas, J. M. *Angew. Chem., Int. Ed.* **1998**, *27*, 1673.
(19) Gates, B. C. *Chem. Rev.* **1995**, *95*, 511.
(20) *Model Systems in Catalysis. Single Crystals to Supported Enzyme Mimics*; Rioux, R., Ed.; Springer: New York, 2010.
(21) de Silva, N.; Ha, J. H.; Solovyov, A.; Nigra, M. M.; Ogino, I.; Yeh, S. W.; Durkin, K. A.; Katz, A. *Nat. Chem.* **2010**, *2*, 1062.
(22) Brown, M. A.; Carrasco, E.; Sterrer, M.; Freund, H. J. *J. Am. Chem. Soc.* **2010**, *132*, 4064.
(23) Mondloch, J. E.; Wang, Q.; Frenkel, A. I.; Finke, R. G. *J. Am. Chem. Soc.* **2010**, *132*, 9701.
(24) Vajda, S.; Pellin, M. J.; Greeley, J. P.; Marshall, C. L.; Curtiss, L. A.; Ballentine, G. A.; Elam, J. W.; Catillon-Mucherie, S.; Redfern, P. C.; Mehmood, F.; Zapol, P. *Nat. Mat.* **2009**, *8*, 213.
(25) Choi, M.; Wu, Z.; Iglesia, E. *J. Am. Chem. Soc.* **2010**, *132*, 9129.

(26) Uzun, A.; Gates, B. C. *Angew. Chem., Int. Ed.* **2008**, *47*, 9245.
(27) Uzun, A.; Gates, B. C. *J. Am. Chem. Soc.* **2009**, *131*, 15887.
(28) Uzun, A.; Ortalan, V.; Browning, N. D.; Gates, B. C. *J. Catal.* **2010**, *269*, 318.
(29) Uzun, A.; Bhirud, V. A.; Kletnieks, P. W.; Haw, J. F.; Gates, B. C. *J. Phys. Chem. C.* **2007**, *111*, 15064.
(30) Miessner, H.; Burkhardt, I.; Gutschick, D.; Zecchina, A.; Morterra, C.; Spoto, G. *J. Chem. Soc., Faraday Trans.* **1989**, *85*, 2113.
(31) Knözinger, E.; Jacob, K.-H.; Singh, S.; Hofmann, P. *Surf. Sci.* **1993**, *290*, 388.
(32) Bonati, F.; Ugo, R. *J. Org. Chem.* **1968**, *11*, 341.
(33) Strohmeier, W.; Müller, F. J. *Chem. Ber.* **1967**, *100*, 2812.
(34) Huheey, J. E.; Keiter, E. A.; Keiter, R. L. *Inorganic Chemistry Principles of Structure and Reactivity*, 4th ed.; Harper Collins: New York, 1993.
(35) Alexeev, O. S.; Kim, D.-W.; Gates, B. C. *J. Mol. Catal. A: Chem.* **2000**, *162*, 67.
(36) Uzun, A.; Dixon, D. A.; Gates, B. C. *ChemCatChem* **2011**, *3*, 95.
(37) Braga, D.; Grepioni, F.; Byrne, J. J.; Calhorda, M. J. *J. Chem. Soc., Dalton Trans.* **1995**, *20*, 3287.
(38) Alley, W. M.; Hamdemir, I. K.; Wang, Q.; Frenkel, A. I.; Li, L.; Yang, J. C.; Menard, L. D.; Nuzzo, R. G.; Ozkar, S.; Johnson, K. A.; Finke, R. G. *Inorg. Chem.* **2010**, *49*, 8131.
(39) Ortalan, V.; Uzun, A.; Gates, B. C.; Browning, N. D. *Nat. Nanotech.* **2010**, *5*, 506.
(40) Bennett, M. A.; Milner, D. A. *J. Am. Chem. Soc.* **1969**, *91*, 6983.
(41) Conner, W. C.; Falconer, J. L. *Chem. Rev.* **1995**, *95*, 759.
(42) Gross, A. *Appl. Phys. A: Mater. Sci. Process.* **1998**, *67*, 627.
(43) Vaska, L.; Werneke, M. F. *Ann. N. Y. Acad. Sci.* **1971**, *172*, 546.
(44) Young, J. F.; Osborn, J. A.; Jardine, F. A.; Wilkinson, G. Hydride *J. Chem. Soc., Chem. Commun.* **1965**, *7*, 131.
(45) Kamer, P. C. J.; van Leeuwen, P. W. N. M.; Reek, J. N. H. *Acc. Chem. Res.* **2011**, *34*, 895.
(46) Sachtler, W. M. H. *Acc. Chem. Res.* **1993**, *26*, 383.
(47) Gallezot, P. *Catal. Rev — Sci. Eng.* **1979**, *20*, 121.
(48) Dalla Betta, R. A.; Boudart, M. In *Proceedings of the 5th International Congress on Catalysis*; Hightower, H., Ed.; Elsevier: Amsterdam, The Netherlands, 1973.
(49) Hadjiivanov, K. I.; Vayssilov, G. N. *Adv. Catal.* **2002**, *47*, 307.
(50) Conner, W. C.; Teichner, S. J.; Pajonk, G. M. In *Advances in Catalysis*; Eley, D. D.; Pines, H.; Weisz, P. B., Eds.; Academic Press: San Diego, 1986; Vol. 34; p 1.
(51) Wiese, K.-D.; Obst, D. *Top. Organomet. Chem.* **2006**, *18*, 1.
(52) Preti, C.; Tosi, G. Z. *Anorg. Allg. Chem.* **1976**, *419*, 185.
(53) Preti, C.; Tosi, G. Z. *Anorg. Allg. Chem.* **1977**, *432*, 259.
(54) Empsall, H. D.; Hyde, E. M.; Mentzer, E.; Shaw, B. L.; Uttley, M. F. *J. Chem. Soc., Dalton Trans.* **1976**, 2069.
(55) Horiuti, J.; Polanyi, M. *Trans. Faraday Soc.* **1934**, *30*, 1164.
(56) Bhirud, V. A.; Uzun, A.; Kletnieks, P. W.; Craciun, R.; Haw, J. F.; Dixon, D. A.; Olmstead, M. M.; Gates, B. C. *J. Organomet. Chem.* **2007**, *692*, 2107.
(57) Jentoft, R. E.; Deutsch, S. E.; Gates, B. C. *Rev. Sci. Instrum.* **1996**, *67*, 2111.
(58) Newville, M.; Ravel, B.; Haskel, D.; Rehr, J. J.; Stern, E. A.; Yacoby, Y. *Physica B* **1995**, *208/209*, 154.
(59) Newville, M. *J. Synchrotron Rad.* **2001**, *8*, 96.
(60) Vaarkamp, M.; Linders, J. C.; Koningsberger, D. C. *Physica B* **1995**, *209*, 159.
(61) Koningsberger, D. C.; Mojet, B. L.; van Dorssen, G. E.; Ramaker, D. E. *Top. Catal.* **2000**, *10*, 143.
(62) Zabinsky, S. E.; Rehr, J. J.; Ankudinov, A.; Albers, R. C.; Eller, M. J. *Phys. Rev. B* **1995**, *52*, 2995.
(63) Pearson, W. B.; Calvert, L. D.; Villars, P. *Pearson's Handbook of Crystallographic Data for Intermetallic Phases*; American Society for Metals: Metals Park, OH, 1985.
(64) Lytle, F. W.; Sayers, D. E.; Stern, E. A. *Physica B* **1989**, *158*, 701.